

# Construction of Crystalline 2D Covalent Organic Frameworks with Remarkable Chemical (Acid/Base) Stability via a Combined Reversible and Irreversible Route

Sharath Kandambeth,<sup>†</sup> Arijit Mallick,<sup>†</sup> Binit Lukose,<sup>‡</sup> Manoj V. Mane,<sup>†</sup> Thomas Heine,<sup>‡</sup> and Rahul Banerjee<sup>\*†</sup>

<sup>†</sup>Physical/Materials Chemistry Division, CSIR-National Chemical Laboratory, Dr. Homi Bhabha Road, Pune 411008, India

<sup>‡</sup>Center for Functional Nanomaterials, School of Engineering and Science, Jacobs University Bremen, Research III, Room 61, Campus Ring 1, 28759 Bremen, Germany

## Supporting Information

**ABSTRACT:** Two new chemically stable [acid and base] 2D crystalline covalent organic frameworks (COFs) (**TpPa-1** and **TpPa-2**) were synthesized using combined reversible and irreversible organic reactions. Syntheses of these COFs were done by the Schiff base reactions of 1,3,5-triformylphloroglucinol (**Tp**) with *p*-phenylenediamine (**Pa-1**) and 2,5-dimethyl-*p*-phenylenediamine (**Pa-2**), respectively, in 1:1 mesitylene/dioxane. The expected enol–imine (OH) form underwent irreversible proton tautomerism, and only the keto–enamine form was observed. Because of the irreversible nature of the total reaction and the absence of an imine bond in the system, **TpPa-1** and **TpPa-2** showed strong resistance toward acid (9 N HCl) and boiling water. Moreover, **TpPa-2** showed exceptional stability in base (9 N NaOH) as well.

Covalent organic frameworks (COFs) are lightweight, porous crystalline materials constructed via strong covalent bonds between elements such as C, B, O, N, and Si.<sup>1</sup> Because of their low densities and  $\pi$ – $\pi$  stacked architectures, COFs have been used as effective gas storage media,<sup>2</sup> catalytic supports,<sup>3</sup> and semiconductive and photoconductive devices.<sup>4</sup> It is believed that reversibility in covalent bond formation during synthesis is required for the successful crystallization of COFs,<sup>5</sup> which is necessary to identify their specific structural details precisely. Irreversible organic reactions always lead to the formation of amorphous porous polymeric materials, separately categorized as porous organic polymers (POPs)<sup>6</sup> or porous aromatic frameworks (PAFs).<sup>7</sup> Even though most POPs and PAFs have high thermal and chemical stability, they are amorphous in nature and do not have any internal ordering. To date, four reversible organic reactions, namely, boronic acid trimerization,<sup>1a</sup> boronate ester formation,<sup>1a</sup> trimerization of nitriles,<sup>1d</sup> and Schiff base reaction,<sup>8</sup> have been used for the synthesis of crystalline COFs. Since reversible back-reactions can occur after the synthesis, COFs in general completely decompose even in the presence of ambient humidity.<sup>9</sup> Small improvements in the water stability have been achieved by pyridine doping<sup>9c</sup> and alkylation<sup>9a</sup> of the COF pore walls. However, these modifications always lead to a decrease in the gas adsorption properties, even though they enhance the hydrolytic stability to a small extent. Hence, the

COF instability problem still remains a challenge that prevents the usage of COFs for diverse practical applications.

Here we report the first synthesis of two new COFs, **TpPa-1** and **TpPa-2**, by a combination of reversible and irreversible organic reactions. They were synthesized by the reaction of 1,3,5-triformylphloroglucinol (**Tp**) with *p*-phenylenediamine (**Pa-1**) or 2,5-dimethyl-*p*-phenylenediamine (**Pa-2**), respectively. The total reaction can be divided into two steps (Figure 1): In the first step, a reversible Schiff base reaction leads to the formation of a crystalline framework, and the second step is an irreversible enol-to-keto tautomerization, which enhances the chemical stability. The irreversible nature of the tautomerism does not affect the crystallinity of the COF, since the transformation involves only shifting of bonds while keeping the atomic positions almost same. **TpPa-1** and **TpPa-2** showed exceptional resistance toward boiling water and acid treatment, and **TpPa-2** also showed exceptional stability in a basic medium (9 N NaOH). Both COFs retained their crystallinity and gas adsorption properties under these conditions.

The syntheses of **TpPa-1** and **TpPa-2** were carried out by the Schiff-base reactions of **Tp** (63 mg, 0.3 mmol) with **Pa-1** (48 mg, 0.45 mmol) and **Pa-2** (61 mg, 0.45 mmol), respectively, in the presence of 3 M acetic acid (0.5 mL) using 1:1 mesitylene/dioxane (3 mL) as the solvent. The powder X-ray diffraction (PXRD) patterns of **TpPa-1** and **TpPa-2** exhibited an intense peak at 4.7°, corresponding to the reflection from the (100) plane (Figure 2a). Minor peaks also appeared at  $2\theta = 8.3, 11.1,$  and 27° for **TpPa-1** and 7.9, 10.9, and 26.5° for **TpPa-2** [Figures S1 and S3 in the Supporting Information (SI)]. The last peak in the PXRD patterns of **TpPa-1** and **TpPa-2** is due to the reflection from the (001) plane. The corresponding  $\pi$ – $\pi$  stacking distances between COF layers were calculated to be 3.3 and 3.6 Å from the *d* spacings between 001 planes. To elucidate the structure of these COFs and calculate the unit cell parameter, two possible two-dimensional (2D) models with eclipsed and staggered stacking were built using self-consistent-charge density functional tight-binding (SCC-DFTB) method.<sup>10</sup> The experimental PXRD patterns matched well with the simulated patterns obtained using the eclipsed stacking model (Figures S1 and S3). Hence, we propose structures close to the

Received: August 21, 2012

Published: November 15, 2012

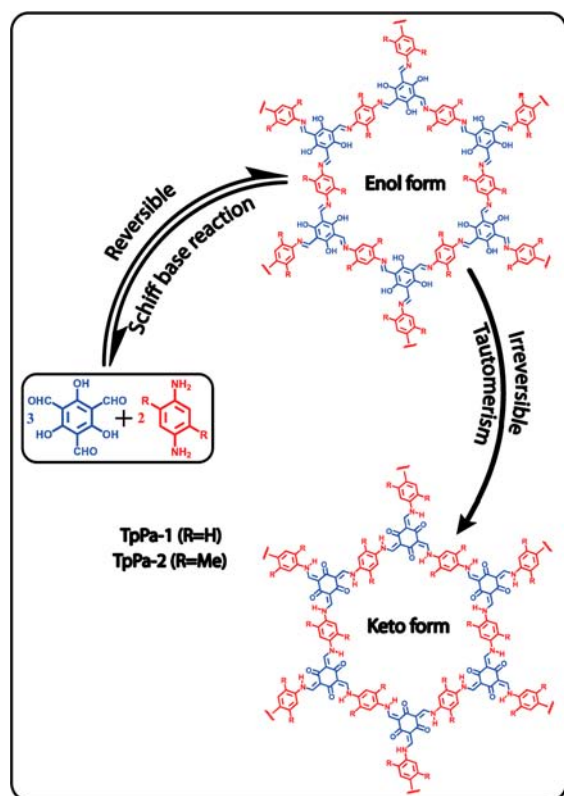


**Figure 1.** Schematic representation of the synthesis of **TpPa-1** and **TpPa-2** by the combined reversible and irreversible reaction of 1,3,5-triformylphloroglucinol with *p*-phenylenediamine and 2,5-dimethyl-*p*-phenylenediamine, respectively. The total reaction proceeds in two steps: (1) reversible Schiff-base reaction and (2) irreversible enol-to-keto tautomerism.

hexagonal space group *P6/m* for **TpPa-1** (Figure 2a) and **TpPa-2** by comparing the experimental PXRD patterns with the simulated ones. To find out the unit cell parameters, Pawley refinements were done for both COFs (section S3 in the SI), which gave the values  $a = b = 22.82 \text{ \AA}$ ,  $c = 3.34 \text{ \AA}$  for **TpPa-1** and  $a = b = 24.52 \text{ \AA}$ ,  $c = 3.63 \text{ \AA}$  for **TpPa-2**.

The FT-IR spectra of **TpPa-1** and **TpPa-2** indicated total consumption of the starting materials on the basis of the disappearance of the N–H stretching bands of **Pa-1** ( $3100\text{--}3300 \text{ cm}^{-1}$ ) and the carbonyl stretching bands of **Tp** ( $1639 \text{ cm}^{-1}$ ) (Figure 2b). Interestingly the FT-IR spectra did not show the characteristic stretching bands of hydroxyl (–OH) or imine (C=N) functional groups, which should have been present if the compounds existed in the enol form. Instead, they showed a strong peak at  $1578 \text{ cm}^{-1}$  arising from the C=C stretching present in the keto form, similar to the peak at  $1578 \text{ cm}^{-1}$  in the FT-IR spectrum of the reference compound 2,4,6-tris-[(phenylamino)methylene]cyclohexane-1,3,5-trione. Most of the FT-IR peaks of **TpPa-1** and **TpPa-2** matched well with those of the reference compound, which exists in the keto form (Figure 2b). However, because of the peak broadening in the extended structure, the C=O peaks of **TpPa-1** and **TpPa-2** at  $1616 \text{ cm}^{-1}$  were merged with the C=C stretching band at  $1578 \text{ cm}^{-1}$  and appeared as a shoulder (Figure S8). The decreased value of the C=O stretching frequency in the reference compound ( $1616 \text{ cm}^{-1}$ ) is due to the strong intramolecular hydrogen bonding and extended conjugation in the structure. The superior intensity of the C=C stretching band is due to the

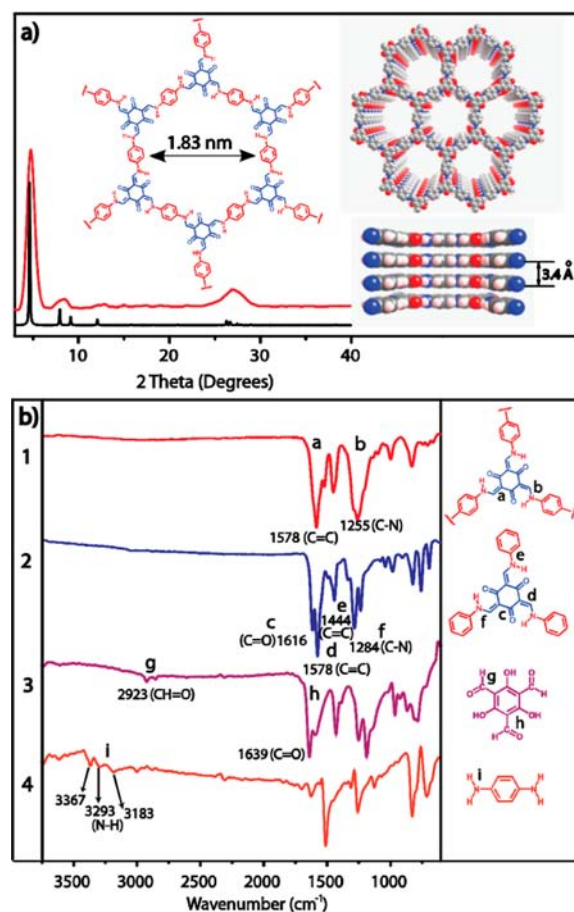


**Figure 2.** (a) Comparison of the observed (red) and simulated (black) PXRD patterns of **TpPa-1**. (b) Comparison of the FT-IR spectra of (1) **TpPa-1**, (2) the reference compound 2,4,6-tris-[(phenylamino)methylene]cyclohexane-1,3,5-trione, (3) **Tp**, and (4) **Pa-1**.

*s-cis* structure. The FT-IR spectrum of **TpPa-2** shows an extra peak at  $2885 \text{ cm}^{-1}$ , which is due to methyl-group C–H stretching.

The isolation of **TpPa-1** and **TpPa-2** in the keto form was unambiguously confirmed by  $^{13}\text{C}$  cross-polarization magic-angle-spinning (CP-MAS) solid-state NMR spectroscopy (Figure 3a). Both COFs showed a clear signal near 180 ppm ( $182 \text{ ppm}$  for **TpPa-1** and  $181.8 \text{ ppm}$  for **TpPa-2**), corresponding to the carbonyl carbons. In the starting material, the aldehyde carbonyl carbon resonance is located downfield near  $192 \text{ ppm}$  (Figure S10). The absence of the peak at  $192 \text{ ppm}$  in the  $^{13}\text{C}$  CP-MAS NMR spectrum indicated the total consumption of the starting materials. The methylated COF (**TpPa-2**) showed an extra peak at  $14 \text{ ppm}$  corresponding to the methyl carbon atoms. Scanning electron microscopy (SEM) images (Figure 3b,d) showed that **TpPa-1** and **TpPa-2** crystallize with a flowerlike morphology, which is a new type of morphology seen in COFs. Each individual flower can be considered as the result of aggregation of a large number of petals with lengths in the micrometer range ( $1\text{--}3 \text{ }\mu\text{m}$ ). In the case of **TpPa-1**, the petals ( $70\text{--}150 \text{ nm}$  wide and  $30\text{--}40 \text{ nm}$  thick) have spike-shaped tips and grow out from a core. In the case of **TpPa-2**, the petals ( $500\text{--}800 \text{ nm}$  wide and  $40\text{--}60 \text{ nm}$  thick) are much broader and longer, forming a platelike structure. The same flower-type morphology was also observed in the transmission electron microscopy (TEM) images, which indicated that

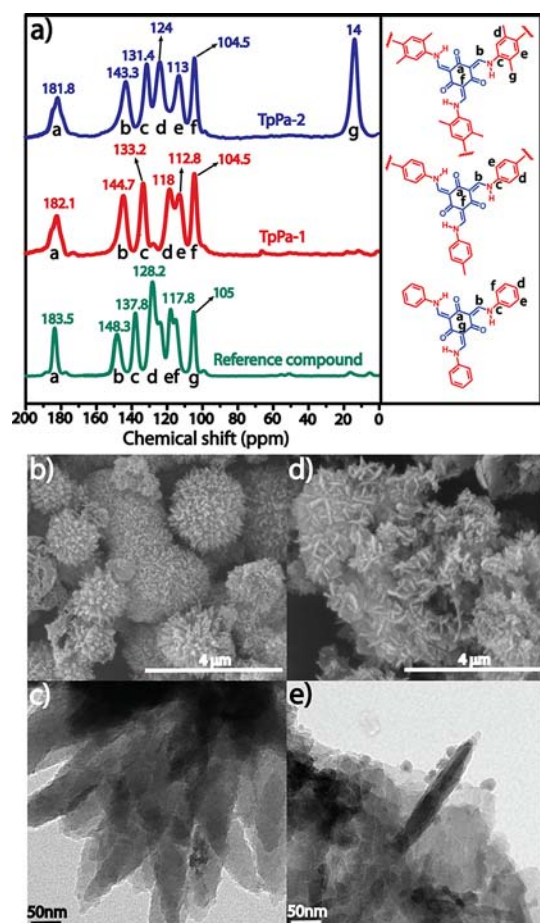


**Figure 3.** (a) Comparison of the  $^{13}\text{C}$  CP-MAS solid-state NMR spectra of **TpPa-1** (red), **TpPa-2** (blue), and the reference compound 2,4,6-tris[(phenylamino)methylene]cyclohexane-1,3,5-trione (green). (b, d) SEM and (c, e) TEM images of (b, c) **TpPa-1** and (d, e) **TpPa-2** showing the nanoflower morphology.

individual petals have a sheetlike structure (Figure 3c,e) that could be formed as a result of  $\pi$ - $\pi$  stacking of COF layers.

Thermogravimetric analysis (TGA) of activated **TpPa-1** and **TpPa-2** was performed to determine their thermal stabilities and confirm the absence of guest molecules inside the pores (Figures S23 and S25). Both COFs showed thermal stability up to 350 °C. Gradual weight losses of 40% for **TpPa-1** and 50% for **TpPa-2** were observed above 360 °C, corresponding to decomposition of the frameworks. The permanent porosities of **TpPa-1** and **TpPa-2** were evaluated by measuring  $\text{N}_2$  adsorption isotherms at 77 K. Activated **TpPa-1** and **TpPa-2** showed reversible type-I adsorption isotherms (Figure S12). The Brunauer–Emmett–Teller (BET) surface areas of the activated COFs were found to be 535  $\text{m}^2/\text{g}$  for **TpPa-1** and 339  $\text{m}^2/\text{g}$  for the methylated COF **TpPa-2** (Figures S14 and S16). **TpPa-1** had a higher Langmuir surface area of 815  $\text{m}^2/\text{g}$ , whereas for **TpPa-2** it was 507  $\text{m}^2/\text{g}$  (Figures S13 and S15). The pore size distributions of **TpPa-1** and **TpPa-2** were calculated on the basis of nonlocal density functional theory (NLDFT). Both COFs had narrow pore size distributions of 0.8–1.5 nm, with peak maxima at 1.25 nm for **TpPa-1** and 1.35 nm for **TpPa-2** (Figures S17 and S18). The hydrogen uptakes of **TpPa-1** and **TpPa-2** were found to be 1.1 and 0.89 wt %, respectively (Figure S19). These values are comparable to the performance of other reported COFs (COF-5, 0.84 wt %; COF-10, 0.82 wt %; COF-102, 1.21 wt %; COF-103,

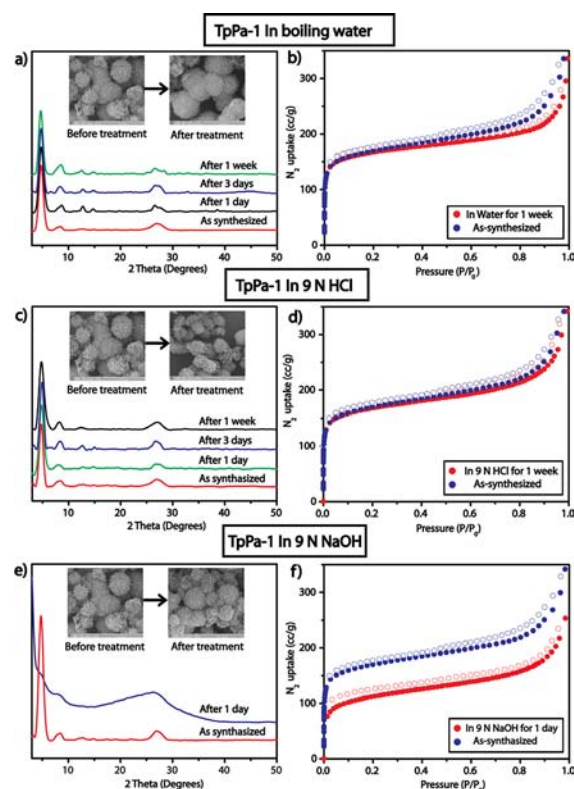


**Figure 4.** Stability tests of **TpPa-1** in (a, b) boiling water, (c, d) 9 N HCl, and (e, f) 9 N NaOH: (a, c, e) PXRD patterns and (b, d, f)  $\text{N}_2$  adsorption isotherms at 77 K (blue) before and (red) after treatment. The insets in (a, c, e) show SEM images before and after treatment.

1.29 wt %).<sup>2</sup> The  $\text{CO}_2$  uptake of **TpPa-1** was measured as 78  $\text{cm}^3/\text{g}$  at 273 K, which is comparable to the performance of COF-6 (85  $\text{cm}^3/\text{g}$ ).<sup>2</sup> **TpPa-2** showed a moderate  $\text{CO}_2$  uptake of 64  $\text{cm}^3/\text{g}$  at the same temperature.

To investigate stability of **TpPa-1** and **TpPa-2** in water, 50 mg of each COF was directly submerged in 10 mL water for 7 days. To our surprise, both COFs remained stable under these conditions. Retention of crystallinity was tested by PXRD (Figure 4a and Figure S37). It was found that the relative peak intensities and peak positions of both COFs remained same after water treatment for 1, 3, and 7 days, which indicates their remarkable water stability. All of the characteristic FT-IR peaks remained same after water treatment, and no extra peaks corresponding to the starting materials were observed. The  $\text{N}_2$  adsorption isotherms (Figure 4b and Figure S38) showed only small decreases in BET surface area (to 520  $\text{m}^2/\text{g}$  for **TpPa-1** and 321  $\text{m}^2/\text{g}$  for **TpPa-2**). Since the COFs showed remarkable stability in water, we decided to check the effect of acid on these materials. The acid stabilities of **TpPa-1** and **TpPa-2** were checked using HCl solutions with different normalities (1, 3, 6, and 9 N) for 1 day. PXRD measurements after the acid treatment indicated high resistance toward acid for both COFs, as their relative peak intensities and peak positions remained same even after treatment with 9 N HCl for 1, 3, and 7 days (Figure 4c and Figure S39). Similarly, the FT-IR peaks remained in the same positions after the acid treatment, indicating the chemical stability of these materials toward acid. Porosity and surface area measurements of the acid-treated COFs (Figure 4d and Figure S40) showed only small changes (to 512  $\text{m}^2/\text{g}$  for **TpPa-1** and 318  $\text{m}^2/\text{g}$  for **TpPa-2**). Finally, we evaluated the stabilities of the two COFs in NaOH solutions with different normalities (1, 3, 6,

and 9 N). **TpPa-2** showed retention of the PXRD peak positions after treatment with 9 N NaOH for 7 days (Figure S41). The nearly unchanged surface area (324 m<sup>2</sup>/g; Figure S42) and retention of peaks the FT-IR spectrum confirmed that **TpPa-2** shows considerable resistance toward base. However, **TpPa-1** showed the loss of PXRD peaks on the first day of treatment with 9 N NaOH (Figure 4e), and only 60 wt % of the material was recovered. Even though FT-IR spectroscopy showed the retention of peaks, gas adsorption analysis (Figure 4f) showed a 50% decrease in surface area.

The stabilities of **TpPa-1** and **TpPa-2** in water arise from the irreversible nature of the enol-to-keto tautomerism. This type of tautomerism also exists in simple *N*-salicylideneanilines, where enol form is found to be more stable (section S11 in the SI). Two competing effects decide which form is more stable: (1) aromaticity and (2) the relative base strengths of the imine nitrogen (C=N) over the phenolic oxygen (O-H). In the case of monosubstituted *N*-salicylideneanilines, aromaticity is the dominating factor, so the compounds exist only in the enol form. However, in the case of tris(*N*-salicylideneaniline) derivatives, the basicity of three imine nitrogens dominates over the aromaticity factor, and as a result, the equilibrium shifts completely toward the keto form (section S11 in the SI). The equilibrium does not revert back to the enol form even after heating the sample to very high temperatures,<sup>11</sup> and thus, this transformation can be considered irreversible. **TpPa-1** and **TpPa-2** were found to be stable even in boiling water as a result of this irreversible enol-to-keto tautomerism. The stability toward acid arises from the disappearance of the acid-labile imine (C=N) bond as a result of the irreversible tautomerism. The framework instability of **TpPa-1** under the influence of base is not completely understood. We speculate that at very high pH there is a chance of deprotonation of the secondary nitrogen, which would lead to the back-conversion of the keto form to the enol form. This speculation was supported by a literature report that upon treatment with a strong base such as lithium diisopropylamide, the reference compound 2,4,6-tris[(phenyl-amino)methylene]cyclohexane-1,3,5-trione underwent deprotonation followed by keto-to-enol tautomerism, which was then used for the chelation of BF<sub>3</sub>.<sup>12</sup> To overcome this base instability problem, two bulky methyl groups were positioned near the base-labile secondary nitrogen center (C-N) in **TpPa-2**. This strategy is similar to the 2,5-dimethylation of the terephthalate linkers in MOF-5, which enhanced the hydrolytic stability of MOF-5 in water.<sup>13</sup> As a result of this methylation in **TpPa-2**, the PXRD peak positions of **TpPa-2** were retained after treatment with 9 N NaOH for 7 days, although a small decrease in peak intensities was observed.

In summary, we for the first time have introduces a new protocol for the synthesis of highly acid- and base-stable crystalline covalent organic frameworks. In addition to their conventional properties such as very low density and high thermal stability, the exceptional stability of these materials will make them advantageous over their metal-organic framework (MOF) counterparts. We have also shown that the problem of base stability can be solved to an extent by introducing a bulky alkyl group near the secondary nitrogen center, at the expense of a small decrease in surface area. Even though the gas adsorption properties of these newly prepared COFs are moderate, we believe that increasing the diamine ligand length will give these COFs better surface areas and gas adsorption properties. The sheetlike petals present in these nanomaterials can be utilized as a

support for doping of nanoparticles, which will be useful for catalytic applications.

## ■ ASSOCIATED CONTENT

### Supporting Information

Synthetic procedures, PXRD data, <sup>13</sup>C solid-state NMR spectra, TGA curves, and crystallographic data (CIF). This material is available free of charge via the Internet at <http://pubs.acs.org>.

## ■ AUTHOR INFORMATION

### Corresponding Author

r.banerjee@ncl.res.in

### Notes

The authors declare no competing financial interest.

## ■ ACKNOWLEDGMENTS

This work is dedicated to Professor Gautam R. Desiraju on the occasion of his 60th birthday. S.K. and A.M. acknowledge CSIR (New Delhi, India) for JRF. R.B. acknowledges funding from CSIR (NWP0021 and -22), DST (SR/S1/IC-22/2009), and BRNS (2011/37C/44/BRNS).

## ■ REFERENCES

- (1) (a) Côté, A. P.; Benin, A. I.; Ockwig, N. W.; Matzger, A. J.; O'Keeffe, M.; Yaghi, O. M. *Science* **2005**, *310*, 1166. (b) Hunt, J. R.; Doonan, C. J.; LeVangie, J. D.; Côté, A. P.; Yaghi, O. M. *J. Am. Chem. Soc.* **2008**, *130*, 11872. (c) Dienstmaier, J. F.; Medina, D. D.; Dogru, M.; Knochel, P.; Bein, T.; Heckl, W. M.; Lackinger, M. *ACS Nano* **2012**, *6*, 7234. (d) Kuhn, P.; Antonietti, M.; Thomas, A. *Angew. Chem., Int. Ed.* **2008**, *47*, 3450.
- (2) Furukawa, H.; Yaghi, O. M. *J. Am. Chem. Soc.* **2009**, *131*, 8875.
- (3) Ding, S. Y.; Gao, J.; Wang, Q.; Zhang, Y.; Song, W. G.; Su, C. Y.; Wang, W. *J. Am. Chem. Soc.* **2011**, *133*, 19816.
- (4) (a) Wan, S.; Guo, J.; Kim, J.; Ihee, H.; Jiang, D. *Angew. Chem., Int. Ed.* **2008**, *120*, 8958. (b) Ding, X.; Chen, L.; Honsho, Y.; Feng, X.; Saengsawang, O.; Guo, J.; Saeki, A.; Seki, S.; Irle, S.; Nagase, S.; Parasuk, V.; Jiang, D. *J. Am. Chem. Soc.* **2011**, *133*, 14510.
- (5) Feng, X.; Ding, X.; Jiang, D. *Chem. Soc. Rev.* **2012**, *41*, 6010.
- (6) Rabbani, M. G.; El-Kaderi, H. M. *Chem. Mater.* **2011**, *23*, 1650.
- (7) Ben, T.; Ren, H.; Ma, S.; Cao, D.; Lan, J.; Jing, X.; Wang, W.; Xu, J.; Deng, F.; Simmons, J. M.; Qiu, S.; Zhu, G. *Angew. Chem., Int. Ed.* **2009**, *48*, 9457.
- (8) (a) Uribe-Romo, F. J.; Joseph, R. H.; Furukawa, H.; Klock, C.; O'Keeffe, M.; Yaghi, O. M. *J. Am. Chem. Soc.* **2009**, *131*, 4570. (b) Uribe-Romo, F. J.; Doonan, C. J.; Furukawa, H.; Oisaki, K.; Yaghi, O. M. *J. Am. Chem. Soc.* **2011**, *133*, 11478.
- (9) (a) Lanni, L. M.; Tilford, R. W.; Bharathy, M.; Lavigne, J. J. *J. Am. Chem. Soc.* **2011**, *130*, 11872. (b) Spitler, E.; Giovino, M.; White, S.; Dichtel, W. *Chem. Sci.* **2011**, *2*, 1588. (c) Du, Y.; Mao, K.; Kamakoti, P.; Ravikovitch, P.; Paur, C.; Cundy, S.; Li, Q.; Calabro, D. *Chem. Commun.* **2012**, *48*, 4606.
- (10) (a) Heine, T.; Rapacioli, M.; Patchkovskii, S.; Frenzel, J.; Koester, A. M.; Calaminici, P.; Escalante, S.; Duarte, H. A.; Flores, R.; Geudtner, G.; Goursot, A.; Reveles, J. U.; Vela, A.; Salahub, D. R. *deMon-nano*; Jacobs University Bremen: Bremen, Germany, 2009. (b) Lukose, B.; Kuc, A.; Heine, T. *Chem.—Eur. J.* **2011**, *17*, 2388.
- (11) Chong, J. H.; Sauer, M.; Patrick, B. O.; MacLachlan, M. J. *Org. Lett.* **2003**, *5*, 3823.
- (12) Riddle, J. A.; Lathrop, S. P.; Bollinger, J. C.; Lee, D. *J. Am. Chem. Soc.* **2006**, *128*, 10986.
- (13) Yang, J.; Grzech, A.; Mulder, F. M.; Dingemans, T. J. *Chem. Commun.* **2011**, *47*, 5244.